WORLD JOURNAL OF PHARMACEUTICAL RESEARCH
Coden USA: WJPRAP
Impact Factor 8.63
Volume 15, Issue 15, 1241-1259.
Research Article
ISSN 2277–7105

POLYMER STABILIZED BARIUM TUNGSTATE ($BAWO_4$) NANOPARTICLES FOR ENHANCED PLANT GROWTH AND ANTIFUNGAL ACTIVITY

Sadasivam Narendhran* and A Rishika

Department of Biotechnology, Sri Krishna Arts and Science College, Kuniamuthur, Coimbatore – 641008.

Article Received on 28 June 2026,
Article Revised on 18 July 2026,
Article Published on 01 Aug. 2026,
https://doi.org/10.5281/zenodo.21697847

***Corresponding Author**
Sadasivam Narendhran
Department of Biotechnology, Sri Krishna Arts and Science College, Kuniamuthur, Coimbatore - 641008.

How to cite this Article: Sadasivam Narendhran* and A Rishika. (2026). Polymer Stabilized Barium Tungstate ($BaWO_4$) Nanoparticles For Enhanced Plant Growth And Antifungal Activity. World Journal of Pharmaceutical Research, 15(15), 1241–1259.

ABSTRACT

This study investigates the potential of polymer-encapsulated barium tungstate ($BaWO_4$) nanoparticles (NPs) as an agent for promoting plant growth and suppressing fungal pathogens. $BaWO_4$ nanoparticles were synthesized via a chemical route and coated with polyvinyl pyrrolidone (PVP) and polyethylene glycol (PEG) to enhance their stability and facilitate controlled release. The effects of the coated NPs on seed germination and early growth were evaluated in *Phaseolus vulgaris* and *Linum usitatissimum*, while antifungal activity against *Fusarium oxysporum* and *Verticillium dahliae* was assessed using the agar well diffusion method.. Characterization by X-ray diffraction confirmed the crystalline structure of the nanoparticles, with average crystallite sizes of 192 nm and 180 nm for PVP and PEG-coated $BaWO_4$ nanoparticles, respectively. The polymer-coated $BaWO_4$ NPs significantly enhanced seed germination and early seedling development in both plant species without exhibiting phytotoxic effects. Antifungal tests revealed that water-dispersed $BaWO_4$ NPs exhibited a clear zone of inhibition (10.03 ± 0.15 mm) at 100 mg/mL, whereas DMSO-dispersed NPs showed negligible activity. These findings suggest that polymer-encapsulated $BaWO_4$ nanoparticles have promising applications as nano-enabled fertilizers and antifungal agents in sustainable agriculture.

KEYWORDS: Barium tungstate, PVP, PEG, Antifungal activity, Seed germination,

Phaseolus vulgaris and *Linum usitatissimum*.

1. INTRODUCTION

Nanotechnology has emerged as a transformative tool in modern agriculture, offering innovative solutions for crop improvement, disease management, and nutrient delivery. Nanomaterials, owing to their high surface area-to-volume ratio and tunable physicochemical properties, are increasingly utilized in the formulation of nanofertilizers and agrochemicals (Dhanya Raj *et al*., 2025). Among the various nanomaterials investigated, metal oxide and tungstate-based nanoparticles have attracted considerable interest due to their multifunctionality and cost-effective synthesis. The development of environmentally sustainable nanomaterials for enhancing plant productivity and managing pathogens is a growing focus in agricultural biotechnology (Golla Nagaraju *et al*., 2022).

Barium tungstate ($BaWO_4$), a p-type semiconductor, is known for its catalytic, optical, and electronic properties, and has been explored in various technological applications including microwave dielectric ceramics, oxygen carriers in syngas production, and photovoltaic cells (Jain et al., 2022). More recently, $BaWO_4$ nanoparticles (NPs) have gained attention in biological applications due to their stability, dispersibility, and potential as carriers for active agents (Cao et al., 2014). To improve their compatibility with biological systems, surface modification using biocompatible polymers such as polyvinyl pyrrolidone (PVP) and polyethylene glycol (PEG) is frequently employed (Sherlin Vinita et al., 2022). These polymers enhance nanoparticle stability in aqueous media and facilitate controlled release, making them suitable candidates for agricultural applications (Dongxiao Cui et al., 2018).

The application of nanomaterials in seed treatment and early plant development represents a promising approach to boost germination, nutrient uptake, and disease resistance. In this study, we selected *Phaseolus vulgaris* (common bean) and *Linum usitatissimum* (flax) (Fig 1) as model crops to evaluate the bioefficacy of polymer-coated $BaWO_4$ nanoparticles. *P. vulgaris* is widely cultivated and consumed across continents as a high-protein food source and plays a crucial role in food security, particularly in developing countries (Banerjee and Rajeswari, 2024). The red kidney bean variety is one of the most common types, known for its nutritional richness and adaptability to diverse agroclimatic zones.

Linum usitatissimum, commonly known as flax, is an ancient oilseed crop valued for its omega-3-rich oil and lignocellulosic fiber. It has been cultivated for thousands of years and remains economically important in regions such as India, Canada, and parts of Europe (Dang et al., 2015). Its seeds are rich in alpha-linolenic and linoleic acids, contributing to its functional food and nutraceutical relevance (Hussain et al., 2016). However, both *P. vulgaris* and *L. usitatissimum* are susceptible to seed borne pathogens, including fungal infections that impact seed viability and early growth stages.

In this study, we synthesized $BaWO_4$ nanoparticles and functionalized them with PVP and PEG to assess their influence on seed germination, early growth parameters, and antifungal activity (*F. oxysporum* and *V. dahlia)*. The novelty of this approach lies in combining growth-promoting and antimicrobial functionalities within a single nanoparticle platform, offering a dual benefit in agricultural biotechnology. The outcomes of this research may support the development of multifunctional nanobiomaterials for sustainable crop production and pathogen control.

2 MATERIALS AND METHODS

2.1 Materials

Seeds of *Phaseolus vulgaris* (red kidney bean) and *Linum usitatissimum* (flax) (Fig 1) were procured from a local agricultural supplier in Coimbatore, Tamil Nadu, India. The fungal strain *Fusarium oxysporum* and *Verticillium dahliae* was kindly provided by the Indian Institute of Microbial Technology (IMTECH), Chandigarh, India. All analytical-grade chemicals and reagents, including polyvinyl pyrrolidone (PVP), polyethylene glycol (PEG), barium chloride ($BaCl_2$), and sodium tungstate (Na_2WO_4), were purchased from Sigma-Aldrich Chemicals (India) and used without further purification.

2.2 Methods

2.2.1 Synthesis of $BaWO_4$ nanoparticles

Barium tungstate ($BaWO_4$) nanoparticles were synthesized using a modified microemulsion method as described by Cao et al. (2014). Briefly, 2 M sodium dodecyl sulfate (SDS) was added to a solvent mixture containing 20 mL of Tween-80 and 2 mL of hexane. This solution (designated as Solution A) was heated in a water bath at 70 °C for 1 hour to ensure micelle formation. Solution B was prepared by dissolving 0.4 M sodium tungstate dihydrate ($Na_2WO_4 \cdot 2H_2O$) in 0.6 mL of deionized water. Separately, Solution C was prepared by dissolving 0.4 M barium chloride ($BaCl_2$) in a mixture of 0.564 mL deionized water and 0.036 mL of 0.1 M hydrochloric acid to maintain acidic conditions. Solutions B and C were then sequentially added dropwise to Solution A under vigorous magnetic stirring, resulting in the formation of a white precipitate indicating $BaWO_4$ nanoparticle synthesis. The reaction mixture was continuously stirred for 15 minutes to ensure homogenous nucleation and particle growth. The resulting suspension was transferred into a ceramic crucible and subjected to thermal treatment in a hot air oven at 100 °C for 24 hours. Post-synthesis, the nanoparticles were allowed to cool to room temperature overnight. The synthesized $BaWO_4$ nanoparticles were harvested by centrifugation at 5000 rpm for 15 minutes. The collected pellet was washed thoroughly with ethanol five times to remove unreacted precursors and surfactants. The final product was dried and stored in airtight vials for subsequent characterization and application studies.

2.2.2 Surface modification of $BaWO_4$ with PVP and PEG

For polymer encapsulation (Abdel Moamen et al., 2024), 10 g of purified $BaWO_4$ nanoparticles were dispersed in 100 mL of deionized water using a vortex mixer for 5 minutes. Separately, 1% (w/v) solutions of polyvinyl pyrrolidone (PVP) and polyethylene glycol (PEG) were prepared by dissolving the respective polymers in 20 mL of formamide. The $BaWO_4$ suspension was divided into two equal parts, and each part was added to the corresponding PVP or PEG solution. The mixtures were stirred vigorously on a magnetic stirrer for 30 minutes, followed by vortexing for an additional 15 minutes to ensure uniform coating. The resulting polymer-coated $BaWO_4$ nanoparticles were collected by centrifugation at 5000 rpm for 15 minutes. The pellets were washed three times with methanol to remove excess polymer and formamide residues. The final PVP- and PEG-coated $BaWO_4$ nanoparticles were dried and stored under sterile conditions for subsequent analyses.

2.2.3 Characterization of PVP and PEG coated $BaWO_4$ nanoparticles

FTIR analysis was performed to identify the surface functional groups and to confirm polymer coating on the $BaWO_4$ nanoparticles. The spectra were recorded using an FTIR spectrometer in the range of 4000–400 cm^{-1}. This analysis also helped determine the biomolecular interactions responsible for nanoparticle stabilization and capping. The crystalline phase and structural characteristics of the nanoparticles were investigated using X-ray diffraction analysis (Rigaku MiniFlex 600, Cu Kα radiation, $\lambda = 1.5406$ Å). The diffraction patterns were recorded over a 2θ range of 10°–80°. Crystallite size was estimated using the Debye–Scherrer equation. Elemental composition of the nanoparticles was determined using EDX analysis integrated with a scanning electron microscope. This technique confirmed the presence and relative abundance of barium (Ba), tungsten (W), and oxygen (O) in the nanoparticle samples. The surface morphology, size distribution, and aggregation state of the nanoparticles were examined using SEM (JEOL JSM-6390). Samples were sputter-coated with gold prior to imaging to improve conductivity. SEM imaging also enabled visualization of polymer coating on the nanoparticle surfaces. These combined techniques provided comprehensive insights into the physicochemical characteristics of the $BaWO_4$ nanoparticles and validated the effectiveness of the surface modification with PVP and PEG.

2.2.4 Effect of polymer coated $BaWO_4$ for *Phaseolus vulgaris* and *Linum usitatissimum* germination

The influence of polymer-coated $BaWO_4$ nanoparticles on seed germination and early plant growth was assessed using *Phaseolus vulgaris* (red kidney bean) and *Linum usitatissimum* (flax) as test species. Seeds were first surface-sterilized following the protocol of Mishra et al., (2025) with slight modifications. Briefly, seeds were wrapped in sterile muslin cloth and rinsed under running tap water for 5 minutes. Subsequently, they were immersed in 10% Tween-20 solution and stirred for 5 minutes to remove surface contaminants. The seeds were then rinsed thoroughly with sterile deionized water to eliminate residual surfactant. Further sterilization was performed by immersing the seeds in 70% ethanol for 2 minutes, followed by multiple washes with sterile deionized water to remove ethanol residues. After sterilization, seeds were carefully placed in sterile 90 mm × 15 mm Petri dishes containing four layers of tissue paper, moistened with sterile deionized water and trimmed to fit the plate.

A series of nanoparticle treatments were prepared using PVP and PEG-coated $BaWO_4$ nanoparticles at five concentrations: T1 = 0.2 g/100 mL, T2 = 0.4 g/100 mL, T3 = 0.6 g/100 mL, T4 = 0.8 g/100 mL, and T5 = 1.0 g/100 mL. For each treatment, *P. vulgaris* (12 seeds per plate) and *L. usitatissimum* (12 seeds per plate) were uniformly distributed using sterile forceps. One millilitre of the respective nanoparticle suspension was sprayed onto the seeds twice daily for seven consecutive days. The experiment was conducted in triplicate under controlled laboratory conditions. At the end of the experimental period, root and shoot lengths were measured, and mean values were recorded. Seed germination performance was evaluated using the germination index, which included the relative germination rate and relative root elongation, calculated as follows:

$$Relative\ germination\ rate = \frac{Seeds\ germinated\ in\ test\ sample}{Seeds\ germinated\ in\ control}\ X\ 100$$

$$Relative\ root\ elongation = \frac{Mean\ root\ length\ in\ test\ sample}{Mean\ root\ length\ in\ control}\ X\ 100$$

$$Germination\ index = \frac{Relative\ germinatio\ rate}{Relative\ root\ elongation}\ X\ 100$$

2.2.5 Determination of Antifungal Activity of polymer coated $BaWO_4$ nanoparticle

The antifungal activity of PVP and PEG-coated barium tungstate ($BaWO_4$) nanoparticles was evaluated against *Fusarium oxysporum* and *Verticillium dahliae* using the agar well diffusion method, as described by Priyadharshan et al. (2025) with slight modifications. The fungal strain was cultured in nutrient broth at room temperature (25 ± 2 °C) for 24 hours to achieve optimal growth. Mueller Hinton Agar (MHA) plates were prepared and uniformly inoculated with the fungal suspension using sterile cotton swabs to ensure even distribution. Wells of 6 mm diameter were aseptically punched into the agar using a sterile gel puncher. Each well was filled with 100 µL of PVP or PEG-coated $BaWO_4$ nanoparticle suspensions at concentrations of 25, 50, 75, and 100 mg/mL. A 10 mg/mL amphotericin B solution served as the positive control, while sterile distilled water was used as the negative control. The plates were incubated at room temperature for 24 hours under sterile conditions. Following incubation, the diameter of the zone of inhibition around each well was measured in millimetres using a calibrated ruler. All assays were performed in triplicate, and the mean values were calculated to determine antifungal efficacy.

3 RESULTS

3.1 FTIR Analysis of polymerized $BaWO_4$

FTIR spectroscopy was employed to identify the surface functional groups and confirm the interaction between $BaWO_4$ nanoparticles and the polymeric coatings (PVP and PEG). The characteristic absorption peaks are summarized in Table 1. The FTIR spectrum of PVP-coated $BaWO_4$ nanoparticles exhibited prominent peaks at 2924.09 cm^{-1}, corresponding to the asymmetric C–H stretching vibrations of aliphatic $–CH_2$ groups, which is typical for the polyvinyl framework. A peak at 1689.64 cm^{-1} was attributed to the stretching vibration of the C=O bond from the lactam ring of PVP, while 1597.06 cm^{-1} reflected C=C stretching vibrations. Peaks at 1388.75 cm^{-1} and 1080.14 cm^{-1} are indicative of C–N and C–O stretching vibrations, respectively, confirming the presence of PVP on the nanoparticle surface (Fig 2).

Additional bands in the lower wavenumber region at 794.67 cm^{-1}, 516.92 cm^{-1}, 478.35 cm^{-1}, 447.49 cm^{-1}, and 424.24 cm^{-1} are attributed to Ba–O and W–O bonding vibrations, signifying the successful formation of $BaWO_4$ crystalline framework. For PEG-coated $BaWO_4$ nanoparticles, the absence of the 2924.09 cm^{-1} band confirmed the lack of PVP residues. Similar to PVP-coated nanoparticles, strong peaks at 1689.64 cm^{-1}, 1597.06 cm^{-1}, 1388.75 cm^{-1}, and 1080.14 cm^{-1} were observed, indicating common structural features and confirming polymer interaction. A distinct absorption at 802.39 cm^{-1} and 547.78 cm^{-1} is likely associated with the –C–O–C– stretching of the PEG ether linkages, affirming its successful coating. The characteristic metal-oxygen bond vibrations (Ba–O and W–O) were also observed in PEG-coated samples at 516.92 cm^{-1}, 478.35 cm^{-1}, and 439.77 cm^{-1}, corroborating the structural integrity of the $BaWO_4$ lattice (Fig 2). This observation aligns with findings by Abdel Moamen et al. (2024), who similarly reported distinct absorption bands, in the low-frequency region (~515–480 cm^{-1}) as signatures of metal–oxygen bonds in barium tungstate synthesized via a sol–gel route. These vibrations are indicative of the structural integrity of the $BaWO_4$ framework and are consistent across different synthesis and modification approaches.

3.2 EDX Spectrum of polymerized $BaWO_4$

The elemental composition of polymers coated $BaWO_4$ and to confirm the purity of synthesised nanoparticle are studied using EDX. $BaWO_4$ polymerized with PVP contains 34.44% of Barium, 41.22% of Tungsten, 18.30% of Oxygen and 6.04% of Carbon. In case of $BaWO_4$ polymerized with PEG it was found that Barium was present at 27.56%, Tungsten was present at 41.22%, Oxygen at 18.30% and Carbon was present at 19.66%. The energy dispersion in the EDX spectrum reflects the strong signals and high peaks of Ba and W and that confirms the nanoparticle is Barium tungstate. These results are in good agreement with the elemental trends observed by Hota et al. (2023), who emphasized that the EDX profiles of barium-based tungstates typically show a strong dominance of Ba and W peaks, confirming their stoichiometric incorporation into the tungstate framework.

3.3 XRD Analysis of polymerized $BaWO_4$

The crystalline structure of the synthesized barium tungstate ($BaWO_4$) nanoparticles coated with polyvinyl pyrrolidone (PVP) and polyethylene glycol (PEG) was investigated using X-ray diffraction (XRD). Both samples exhibited characteristic diffraction peaks corresponding to the tetragonal phase of $BaWO_4$, consistent with the standard JCPDS card No. 43-0646.

Prominent diffraction peaks were observed at 2θ values around 17.5°, 28.2°, 32.0°, 43.1°, and 53.7°, which correspond to the (100), (112), (102), (114), and (204) planes, respectively, confirming the successful formation of crystalline $BaWO_4$ (Fig 4). These characteristic reflections are in agreement with those reported by Zhou et al. (2005), who also identified the tetragonal scheelite-type $BaWO_4$ phase during the synthesis of hollow nanospheres using a polymer micelle-assisted strategy. To evaluate the crystallite dimensions, the Scherrer equation was applied to the major diffraction peaks. The average crystallite size for PVP-coated $BaWO_4$ was estimated to be 192.02 nm, while that of the PEG-coated $BaWO_4$ was slightly smaller at 180.49 nm.

In both PVP- and PEG-coated samples, no additional impurity peaks were detected, indicating high phase purity. However, slight shifts in 2θ values and variations in full width at half maximum (FWHM) were observed between the two coatings, suggesting minor differences in crystallite size and strain, possibly influenced by the nature of the polymer capping agents. In our study, the (112) plane exhibited the highest intensity at ~28.2°, designating it as the preferred orientation for crystal growth, which is consistent with the dominant orientation observed in similar $BaWO_4$ nanostructures by Zhou et al., (2005). The XRD peak broadening indicated nanoscale crystallinity, with sharper peaks observed in the PEG-coated sample, suggesting a marginal increase in crystallite size compared to PVP-coated $BaWO_4$. Overall, both PVP and PEG coatings did not alter the fundamental crystal structure but influenced the degree of crystallinity and peak intensity distribution of $BaWO_4$ nanoparticles.

3.4 SEM Analysis of polymerized $BaWO_4$ nanoparticle

The surface morphology of $BaWO_4$ nanoparticle coated with PVP and $BaWO_4$ nanoparticle coated with PEG were observed under Scanning Electron Microscopy (SEM) under four different magnifications (Fig 5 & 6). The polymerized nanoparticle under four magnifications vividly indicated the nanoparticles were aggregated and ellipse shaped. Comparable morphological features have been reported by Oliveira et al. (2022) in their study of cobalt tungstate ($CoWO_4$) crystals, where he observed irregular, anisotropic, and ellipsoidal morphologies influenced by reaction kinetics and synthesis conditions.

3.5 Effect of polymerised $BaWO_4$ Treatment on *Phaseolus vulgaris and Linum usitatissimum* Germination

The influence of polymer-coated barium tungstate ($BaWO_4$) nanoparticles on the seed germination and early development of *Phaseolus vulgaris* and *Linum usitatissimum* was assessed through root and shoot elongation metrics under varying treatment concentrations. The results, summarized in Figure 7, demonstrate that polymerized nanoparticles did not exhibit adverse effects at lower concentrations and, in some cases, enhanced early plant growth compared to the untreated control.

In *Phaseolus vulgaris*, root growth was largely unaffected or slightly enhanced at lower nanoparticle concentrations, particularly in treatments T1–T4. The maximum root length (14.73 ± 2.26 cm) was recorded for PEG-coated $BaWO_4$ at T3 concentration, whereas the lowest root development (7.83 ± 1.09 cm) was observed with PVP-coated $BaWO_4$ at T5 concentration (Fig 8). Compared to the control (13.53 ± 2.98 cm), both PVP and PEG-coated nanoparticles supported comparable or slightly diminished root elongation at higher concentrations, indicating concentration-dependent phytotoxicity. In *Linum usitatissimum*, shoot and root elongation showed a concentration-dependent trend (Fig 9). PEG-coated $BaWO_4$ nanoparticles consistently supported better shoot growth than PVP-coated ones. The highest shoot length (8.73 ± 1.20 cm) was observed in PEG-coated treatment (T3), exceeding the control (8.06 ± 0.51 cm). Root measurements followed a similar trend, with PEG-coated nanoparticles performing better across most concentrations compared to their PVP counterparts. However, at the highest concentration (T5), significant inhibition in root elongation (0.63 ± 0.70 cm) was recorded for PVP-coated nanoparticles.

A similar trend was reported by Banerjee and Rajeswari (2024), where selenium nanoparticles synthesized using *Moringa oleifera* leaf extract significantly improved the morphological features of Phaseolus vulgaris. Their study highlighted increased chlorophyll, tannin, flavonoid, and phenol content in plants grown under selenium nanoparticle treatment, which correlated with improved growth parameters. The calculated germination indices supported these findings. *Phaseolus vulgaris* exposed to PVP- and PEG-coated $BaWO_4$ nanoparticles showed enhanced germination rates of 113.53% and 109.46%, respectively, relative to the control. For *Linum usitatissimum*, shoot elongation germination indices were 119.04% (PVP) and 106.66% (PEG), while root elongation indices were 83.6% and 59.27%, respectively. These results suggest that both PVP and PEG-coated $BaWO_4$ nanoparticles are effective in promoting early seedling growth at lower concentrations, with PEG-coated nanoparticles demonstrating better biocompatibility and reduced phytotoxicity. However, a concentration-dependent toxicity was observed, especially with PVP coatings at higher levels. Based on the relative germination index, the observed toxicity ranking was PVP > PEG.

3.6 Antifungal Activity

The antifungal potential of PVP and PEG-coated barium tungstate ($BaWO_4$) nanoparticles was evaluated against *Fusarium oxysporum* and *Verticillium dahliae* using the agar well diffusion method. Zones of inhibition (mm) at varying nanoparticle concentrations (25, 50, 75, and 100 mg/mL) were measured and compared with the commercial antifungal agent Amphotericin B (10 µg/mL), used as a positive control (Fig 10).

In the case of *Fusarium oxysporum*, both PVP and PEG-coated $BaWO_4$ nanoparticles exhibited concentration-dependent antifungal activity. The maximum zone of inhibition was observed at 100 mg/mL for both coatings (15.16 ± 0.44 mm), which exceeded the inhibition produced by Amphotericin B (12.83 ± 0.44 mm). Even at the lowest concentration (25 mg/mL), a moderate inhibition zone of 12.83 ± 0.44 mm was recorded for both polymer-coated nanoparticles. For *Verticillium dahliae*, PEG and PVP-coated nanoparticles demonstrated comparable efficacy. At 75 mg/mL, PVP-$BaWO_4$ nanoparticles produced the highest inhibition (14.00 ± 1.52 mm), closely approaching the effect of Amphotericin B (14.83 ± 0.44 mm). PEG-coated nanoparticles also showed consistent inhibition across all concentrations, with values ranging from 12.00 to 14.00 mm. However, a slight decrease in inhibition was observed at 50 mg/mL with both polymers.

Priyadharshan et al. (2025), where $BaWO_4$ nanoparticles synthesized using Citrus limon extract demonstrated significant antifungal and antibacterial activity. The authors attributed this to the generation of reactive oxygen species (ROS) and strong metal-oxide interactions with microbial membranes, a mechanism likely relevant to our polymer-functionalized nanoparticles as well. The antifungal capability of tungstate-based nanomaterials has been supported in previous reports. Waghchaure and Adole (2023) emphasized the broad-spectrum antimicrobial efficacy of plant-mediated metal and metal oxide nanoparticles, pointing out their potential as eco-friendly and efficient alternatives to synthetic fungicides. Although our nanoparticles were not biosynthesized, the inclusion of biocompatible polymers like PVP and PEG aligns with the trend toward safer nanomaterial development.

Moreover, Thilagavathi et al. (2021) and Phuruangrat et al. (2009) highlighted the antimicrobial efficiency of WO_4 and $BaWO_4$ nanostructures, respectively, where structural and surface modifications significantly influenced their bioactivity. This supports our observation that PEG-coated $BaWO_4$ exhibited slightly higher or more consistent antifungal effects than PVP-coated samples, likely due to better surface interaction and polymer compatibility with biological systems. The antifungal performance was also influenced by particle size and morphology, as suggested by Li et al. (2006) and Parhi et al. (2008), who demonstrated that different synthetic routes leading to specific nanocrystal shapes and sizes could drastically alter the biological properties of $BaWO_4$. Our SEM analysis showed ellipsoidal, moderately aggregated structures which may have facilitated enhanced fungal surface contact and activity. The results indicate that $BaWO_4$ nanoparticles coated with PVP and PEG possess strong antifungal activity against both tested pathogens. At higher concentrations (75 and 100 mg/mL), their efficacy was comparable to or greater than that of the commercial antifungal agent. These findings suggest that polymer-coated $BaWO_4$ nanoparticles could serve as promising bioactive agents for fungal pathogen management in agricultural biotechnology.

4. CONCLUSION

This study successfully demonstrated the synthesis, polymeric surface functionalization, and multifunctional applications of barium tungstate ($BaWO_4$) nanoparticles coated with polyvinyl pyrrolidone (PVP) and polyethylene glycol (PEG). Characterization through FTIR, XRD, SEM, and EDX confirmed the structural integrity, polymer interactions, crystallinity, and elemental composition of the coated nanoparticles. FTIR spectra verified distinct polymer-specific bonding, while XRD analysis confirmed the formation of a pure tetragonal $BaWO_4$ phase in both PVP and PEG-coated samples. SEM observations revealed elliptical nanoparticle morphology with moderate aggregation, and EDX spectra validated the elemental purity of the samples. Biological assessments revealed that PEG-coated $BaWO_4$ nanoparticles exhibited superior biocompatibility and plant growth-promoting effects, particularly in enhancing root and shoot development in *Phaseolus vulgaris* and *Linum usitatissimum*. Conversely, PVP-coated nanoparticles showed a higher degree of concentration-dependent phytotoxicity at elevated doses. Germination indices further substantiated the favorable response of both plant species to low- to mid-range nanoparticle treatments, supporting their role as potential nanofertilizers.

Antifungal studies indicated that both PEG and PVP-coated $BaWO_4$ nanoparticles possess robust inhibitory activity against *Fusarium oxysporum* and *Verticillium dahliae*. At concentrations of 75–100 mg/mL, the nanoparticles outperformed or matched the efficacy of amphotericin B, highlighting their potential as alternative biofungicidal agents in crop protection. Collectively, the results underscore the dual functionality of polymer-coated $BaWO_4$ nanoparticles as plant growth enhancers and antifungal agents. Their environmentally friendly nature and efficacy at low concentrations make them attractive candidates for sustainable agricultural biotechnology. Future work should focus on field-scale validation, long-term ecotoxicological assessments, and the exploration of their molecular mode of action in plant-pathogen interactions.

ACKNOWLEDGEMENT

We acknowledge the management of Sri Krishna Arts and Science College, Coimbatore, Tamil Nadu, India for providing necessary facilities to carry out this study.

Declarations

Conflict of interest the authors declare no conflict of interest.

Data Availability

Data will be available from corresponding author on reasonable request.

Statement and Declarations

Funding: The authors declare that no funds, grants, or other support were received during the preparation of this manuscript.

Competing Interests: The authors have no relevant financial

Author Contributions: Author contributed to the study conception and design. Material preparation, data collection and analysis were performed by A. Rishika. The first draft of the manuscript was written by S. Narendhran.

Ethics approval: Not Applicable.

Consent to participate: Not Applicable.

Consent to publish: Not Applicable.

FIGURES

Fig. 1: *Phaseolus vulgaris(a)* and *Linum usitatissimum(b)* seeds respectively.

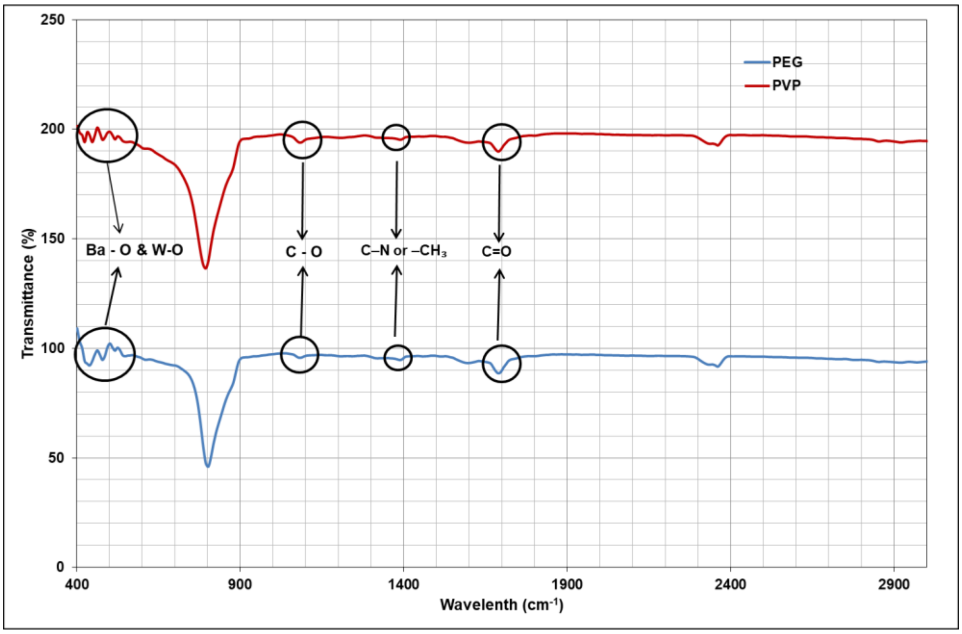

Fig. 2: FTIR Spectrum of polymers coated $BaWO_4$ nanoparticles.

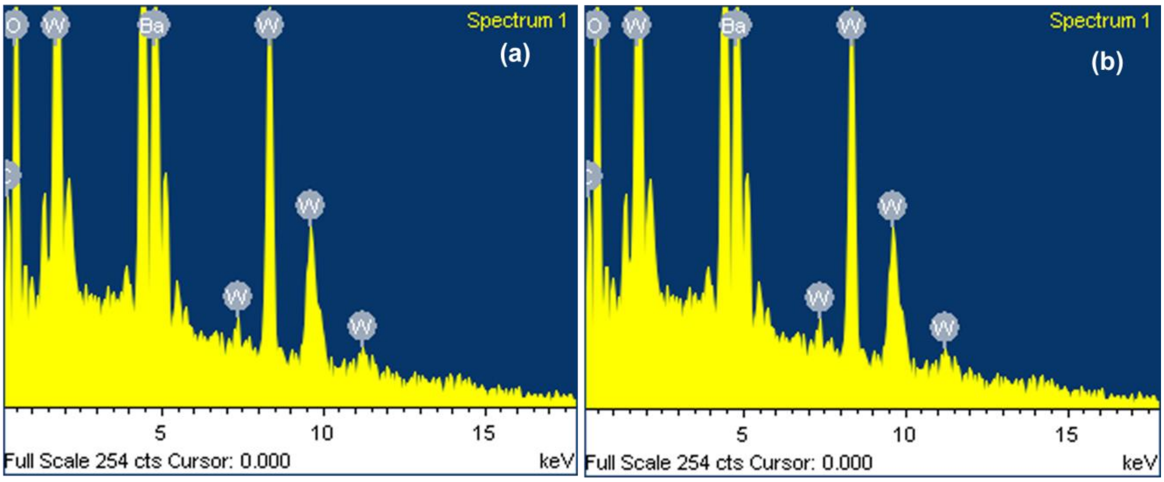

Fig. 3: EDX spectrum of $BaWO_4$ nanoparticle coated with polymers (a) PVP and (b) PEG.

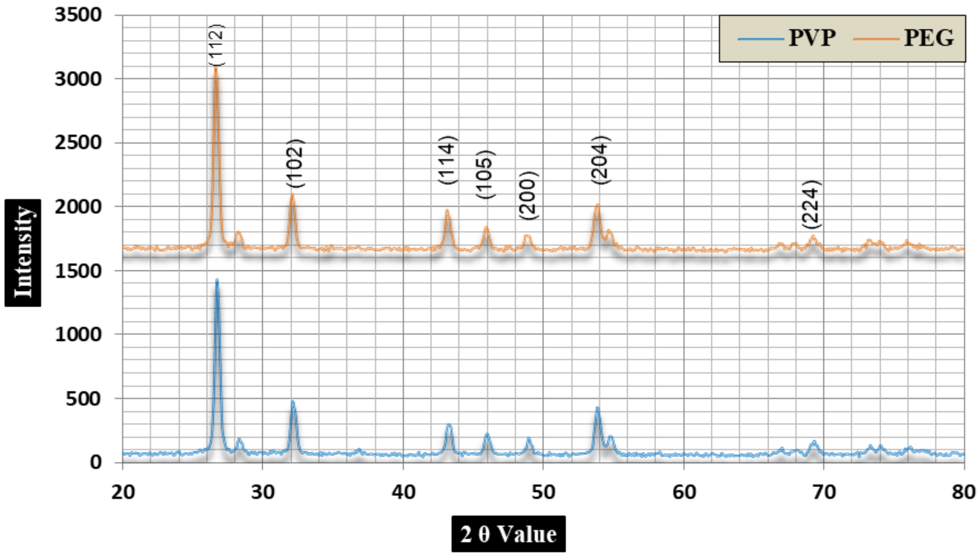

Fig. 4: XRD patterns of polymer coated $BaWO_4$ nanoparticle.

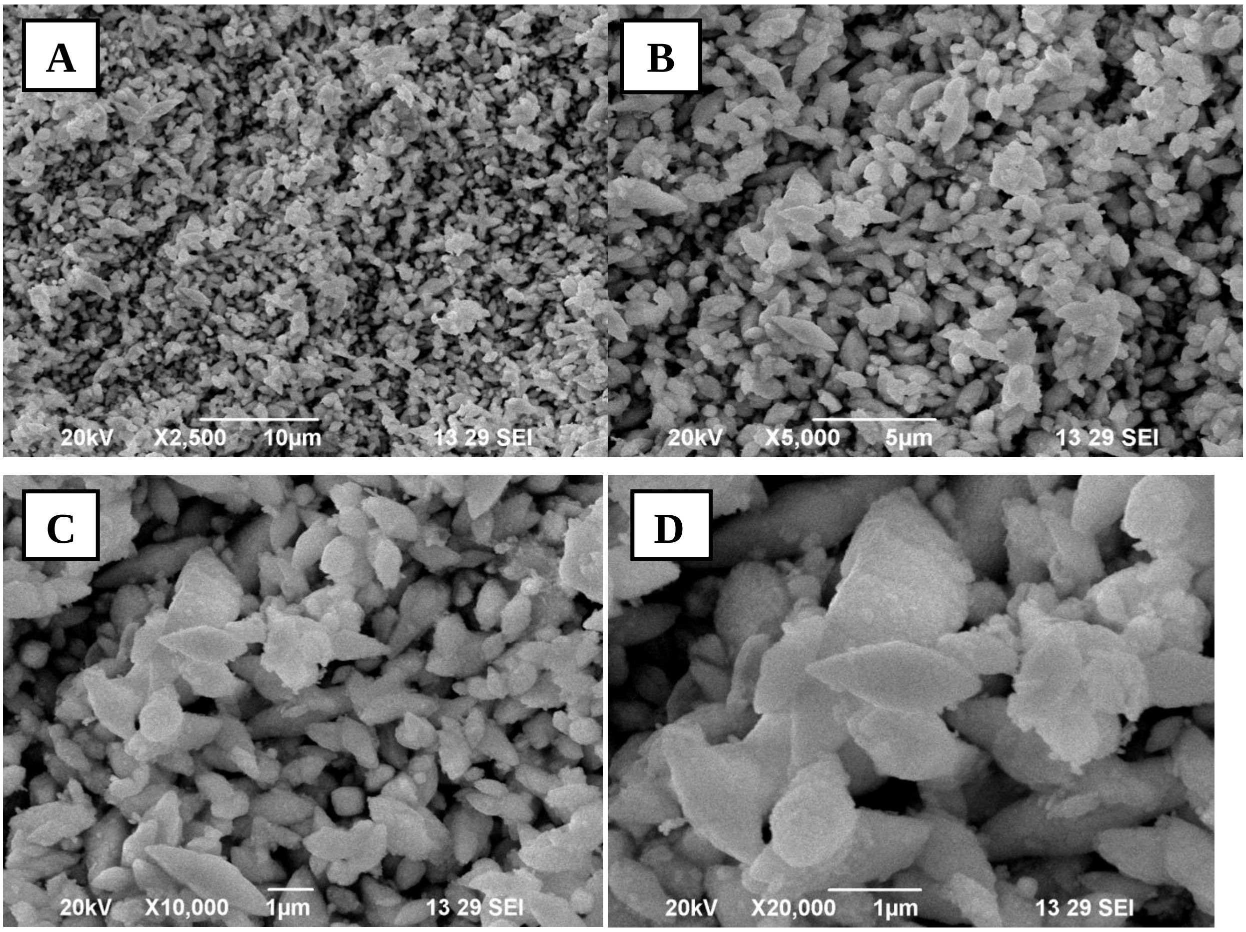

Fig. 5: Scanning electron microscope image of $BaWO_4$ coated with PVP under different magnifications.

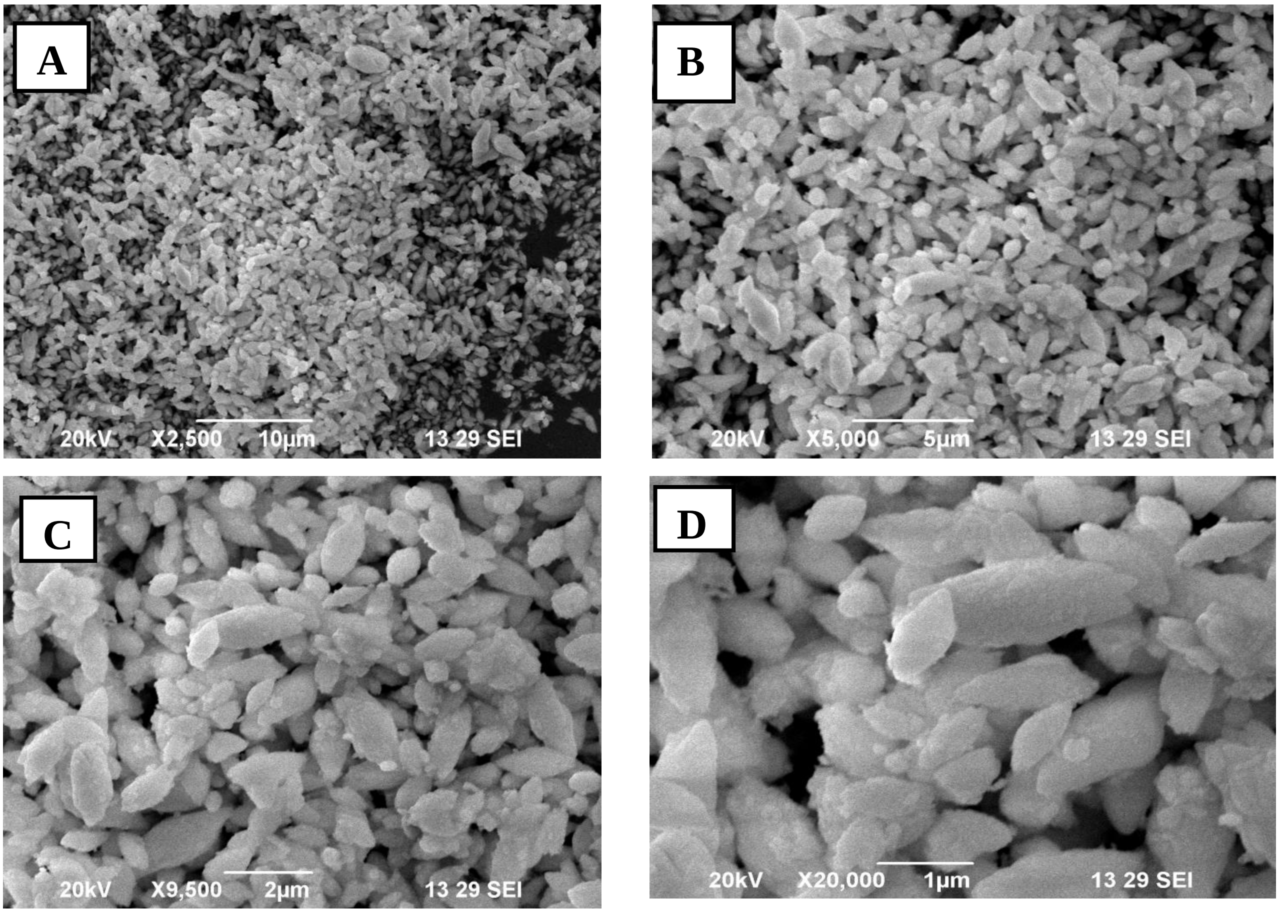

Fig. 6: Scanning electron microscope image of $BaWO_4$ coated with PEG under different magnifications.

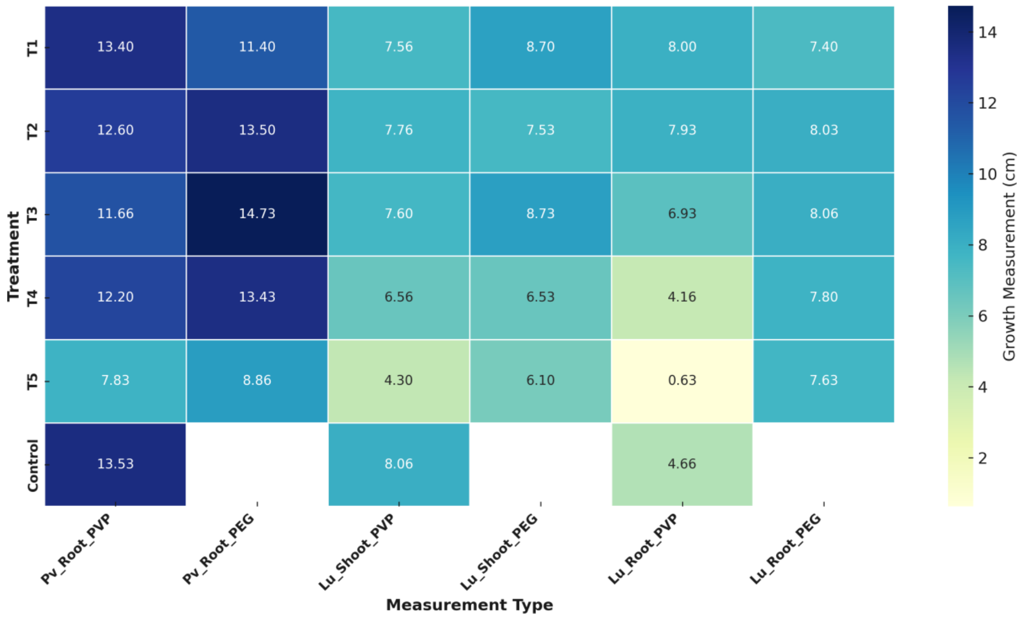

Fig. 7: Heatmap representation of plant growth responses to varying concentrations of PVP- and PEG-coated $BaWO_4$ nanoparticles. Growth parameters include root length of

Phaseolus vulgaris **(Pv_Root), and root and shoot length of *Linum usitatissimum* (Lu_Root, Lu_Shoot). Treatments (T1–T5) correspond to increasing nanoparticle concentrations (0.2–1.0 g/100 mL). Darker shades indicate higher growth values. The control represents untreated seeds. Each value is the mean of three replicates (± SD).**

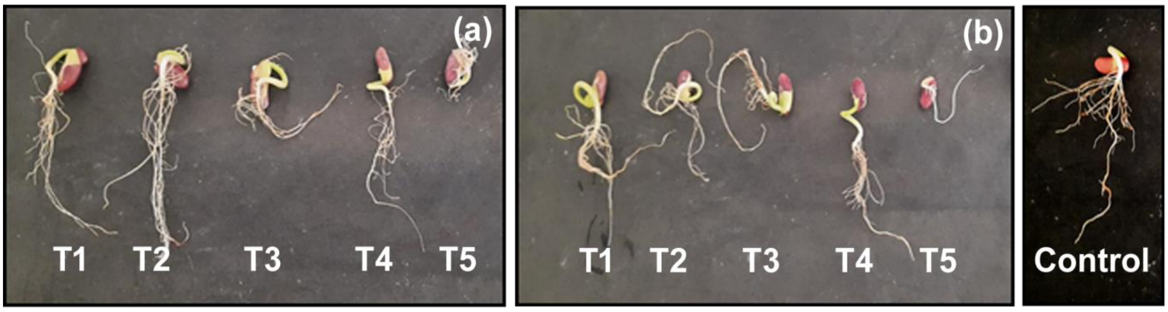

Fig. 8: Seed germination of *Phaseolus vulgaris* using $BaWO_4$ coated with (a) PVP (b) PEG.

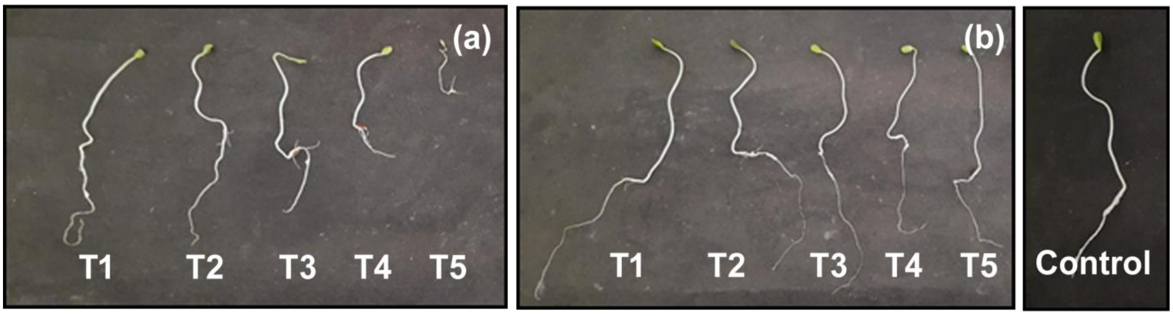

Fig. 9: Seed germination of *Linum usitatissimum* using $BaWO_4$ coated with (a) PVP (b) PEG.

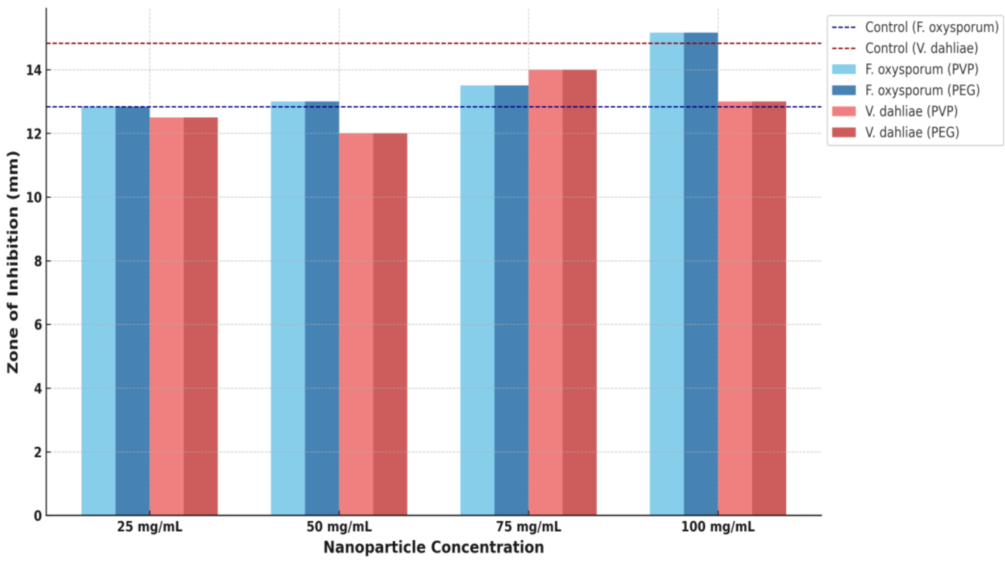

Fig. 10: Comparative antifungal activity of PVP and PEG-coated barium tungstate

($BaWO_4$) nanoparticles against *Fusarium oxysporum* and *Verticillium dahliae*. Zone of inhibition was measured after 24 hours of incubation for nanoparticle concentrations of 25, 50, 75, and 100 mg/mL. Amphotericin B (10 µg/mL) was used as the positive control (dashed lines). Data represent the mean values of triplicates. Both PVP and PEG coatings showed a dose-dependent inhibition with maximal activity observed at 100 mg/mL, comparable to or exceeding the control.

Table 1: FTIR Absorption Peaks (cm^{-1}) of Polymer-Coated $BaWO_4$ Nanoparticles.

Functional group and bond		$BaWO_4$ coated with PVP	$BaWO_4$ coated with PEG
Aliphatic	C-H	2924.09	-
Carbonyl	C=O	1689.64	1689.64
Aromatic or alkene	C=C	1597.06	1597.06
Alkane/Nitrogen	C–N or $–CH_2$	1388.75	1388.75
Ether/Alcohol	C–O	1080.14	1080.14
Ether linkage	–C–O–C–	-	802.39
Metal–oxygen	W–O or Ba–O	794.67	
Polymer–metal	–C–O–M	-	547.78
Metal–oxygen	W–O	516.92	516.92
Metal–oxygen	W–O	478.35	478.35
Metal–oxygen	Ba–O	447.49	439.77
Metal–oxygen	W–O (bending)	424.24	-

Table 2: Elemental analysis through energy dispersion in the EDX spectrum.

ELEMENT	Atomic%				Weight%			
	Ba	W	O	C	Ba	W	O	C
$BaWO_4$ coated with PVP	11.82	10.56	53.91	23.71	34.44	41.22	18.30	6.04
$BaWO_4$ coated with PEG	6.09	5.33	38.89	49.68	27.56	32.29	20.50	19.66

REFERENCE

1. Abdel Moamen OA, Youssef WM, Hagag MS, Masoud AM, Hassanein TF, Taha MH, El-Kamash AM Mechanism insight of sorption of Er(III) and Nd(III) ions onto aluminium barium tungstate synthesized via streamlined sol–gel technique: Time-transient study. Sep Purif Technol, 2024; 344: 127177. https://doi.org/10.1016/j.seppur.2024.127177
2. Banerjee M, Rajeswari VD, Green synthesis of selenium nanoparticles using leaf extract of Moringa oleifera, their biological applications, and effects on the growth of Phaseolus vulgaris – Agricultural synthetic biotechnology for sustainable nutrition. Biocatal Agric Biotechnol, 2024; 55: 102978. https://doi.org/10.1016/j.bcab.2023.102978

3. Cao Y, Zhu K, Liu J, Qiu J. Fabrication of $BaTiO_3$ nanoparticles and its formation mechanism using the high temperature mixing method under hydrothermal conditions. Adv Powder Technol, 2014; 25: 853–858. https://doi.org/10.1016/j.apt.2013.12.012
4. Dang NV, Dung NT, Phong PT, Lee IJ Effect of Fe^{3+} substitution on structural, optical and magnetic properties of barium titanate ceramics. Phys B Condens Matter, 2015; 457: 103–107. https://doi.org/10.1016/j.physb.2014.09.046
5. Dhanya Raj, Manjusha MV, Sapna K, Chandini C Mohan, Sarita G Bhat Anticancer potential of barium titanate nanoparticles: Structural, optical and biomedical perspectives. Results Surf Interfaces, 2025; 20: 100584. https://doi.org/10.1016/j.rsurfi.2025.100584
6. Cui D, Yan C, Miao J, Zhang X, Chen J, Sun L, Meng L, Liang T, Li Q. Synthesis, characterization and antitumor properties of selenium nanoparticles coupling with ferulic acid. Mater Sci Eng C., 2018; 90: 104–112. https://doi.org/10.1016/j.msec.2018.04.048
7. Nagaraju G, Saritha G, Anju TA, Kumar A. Nanotechnology – Big impact: How nanotechnology is changing the future of agriculture? J Agric Food Res., 2022; 10: 100457. https://doi.org/10.1016/j.jafr.2022.100457
8. Hota SS, Panda D, Choudhary RNP Studies of structural, dielectric, and electrical properties of polycrystalline barium bismuth tungstate for thermistor application. Inorg Chem Commun, 2023; 153: 110785. https://doi.org/10.1016/j.inoche.2023.110785
9. Hussain I, Singh NB, Singh A, Singh H, Singh SC Green synthesis of nanoparticles and its potential application. Biotechnol Lett., 2016; 38: 545–560. https://doi.org/10.1007/s10529-015-2026-7
10. Jain A, Wang YG, Shi LN Recent developments in $BaTiO_3$-based lead-free materials for energy storage applications. J Alloys Compd, 2022; 928: 167066. https://doi.org/10.1016/j.jallcom.2022.167066
11. Li D, Wu H, Li Z, Cong X, Sun J, Ren Z, Liu L, Li Y, Fan D, Hao J. Multi-phase equilibrium microemulsions-based routes to synthesize nanoscale $BaWO_4$ spheres, cylinders and rods. Colloids Surf A Physicochem Eng Asp., 2006; 274: 18–23. https://doi.org/10.1016/j.colsurfa.2005.08.033
12. Mishra M, Shukla N, Fatima M, Singh NK Biogenic selenium nanoparticles as nanopriming agents: Promoting germination and strengthening antioxidant defense in rice (Oryza sativa L.). Biocatal Agric Biotechnol, 2025; 65: 103568. https://doi.org/10.1016/j.bcab.2025.103568

13. Oliveira YL, Gouveia AF, Costa MJS, Lopes FHP, Sczancoski JC, Longo E, Luz GE Jr, Santos RS, Cavalcante LS Investigation of electronic structure, morphological features, optical, colorimetric, and supercapacitor electrode properties of $CoWO_4$ crystals. Mater Sci Energy Technol, 2022; 5: 125–144. https://doi.org/10.1016/j.mset.2021.12.006
14. Parhi P, Karthik TN, Manivannan V. Synthesis and characterization of metal tungstates by novel solid-state metathetic approach. J Alloys Compd, 2008; 465: 380–386. https://doi.org/10.1016/j.jallcom.2007.10.089
15. Phuruangrat A, Thongtem T, Thongtem S. Barium molybdate and barium tungstate nanocrystals synthesized by a cyclic microwave irradiation. J Phys Chem Solids, 2009; 70: 955–959. https://doi.org/10.1016/j.jpcs.2009.05.006
16. Priyadharshan M, Karthikeyan M, Rajkumar S, Al Tami MS, Alhomaidi EA. Facile synthesis of $BaWO_4$ nanoparticles using Citrus limon leaf extract: Antibacterial, antifungal, antioxidant, and anticancer activities. J Ind Eng Chem., 2025; 149: 791–800. https://doi.org/10.1016/j.jiec.2025.02.039
17. Vinita SV, et al. Structural, Raman and optical investigations of barium titanate nanoparticles. Phosphorus Sulfur Silicon Relat Elem., 2022; 197: 169–175. https://doi.org/10.1080/10426507.2021.1993850
18. Thilagavathi T, Venugopal D, Thangaraju D, Marnadu R, Palanivel B, Imran M, Shkir M, Ubaidullah M, AlFaify S. A facile co-precipitation synthesis of novel $WO_3/NiWO_4$ nanocomposite with improved photocatalytic activity. Mater Sci Semicond Process, 2021; 133: 105970. https://doi.org/10.1016/j.mssp.2021.105970
19. Waghchaure RH, Adole VA Biosynthesis of metal and metal oxide nanoparticles using various parts of plants for antibacterial, antifungal and anticancer activity: A review. J Indian Chem Soc., 2023; 100: 100987. https://doi.org/10.1016/j.jics.2023.100987
20. Zhou G, Lü M, Xiu Z, Wang S, Zhang H, Zou W. Polymer micelle-assisted fabrication of hollow $BaWO_4$ nanospheres. J Cryst Growth, 2005; 276: 116–120. https://doi.org/10.1016/j.jcrysgro.2004.10.157